Efficient Macro-Micro Scale Coupled Modeling of Batteries

Venkat R. Subramanian,*,z Vinten D. Diwakar,** and Deepak Tapriyal

Department of Chemical Engineering, Tennessee Technological University, Cookeville, Tennessee 38505, USA

In this paper, efficient approximate solutions are developed for microscale diffusion inside porous electrodes. Approximate solutions developed for the microscale diffusion are then coupled with governing equations for the macroscale to predict the electrochemical behavior of a lithium-ion cell sandwich. Approximate solutions developed facilitate the numerical simulation of batteries by reducing the number of differential algebraic equations resulting from the discretization of governing equations.
© 2005 The Electrochemical Society. [DOI: 10.1149/1.2032427] All rights reserved.

Electrochemical models that predict the performance of batteries accurately are usually complex because of the nonlinear coupling of the dependent variables in the governing equations and nonconstant kinetic and transport parameters.[1-4] These models have been used by various researchers to optimize the cell design and to study the effect of system parameters and thermal behavior. These models for porous electrodes involve two scales: electrolyte transport, electrolyte conduction, and solid-phase conduction in the macroscale (x) and solid-state diffusion in the microscale inside the particle (r).

Battery models typically solve electrolyte concentration and electrolyte potential in the separator; and electrolyte concentration, electrolyte potential, solid-state potential, and solid-state concentration in the porous electrode.[1-4] Even when one-dimensional transport in the macroscale (x) is considered, these models involve two coupled nonlinear partial differential equations (PDEs) (in x,t) in the separator and three coupled nonlinear PDEs (in x,t) in the porous electrode.[1-4] In addition, solid-state diffusion should be solved in the pseudodimension (r,t) in the electrode. For predicting the thermal behavior, one has to add an additional equation for temperature. The finite-difference technique[2,3] is the most common technique used for simulation of batteries, though collocation, finite element, and other techniques have also been used by some researchers.[3]

If one has to simulate these battery models rigorously, it would involve discretization of spatial derivatives in the macroscale and also in the microscale. For example, if one were to use 100 node points in the macroscale (x) and 20 node points in the microscale (r), one has to solve $4 \times 100 \times 20 = 8000$ differential algebraic equations resulting from the discretization of the governing equations. Duhamel's superposition theorem was used by Doyle et al.[3] to eliminate the pseudodimension (r). This involves an infinite series and has to be taken care of while integrating macroscale equations numerically in time. This means that one cannot use existing advanced numerical solvers directly for the integration of macroscale equations in time.[2,3] In addition, this method cannot be used for concentration-dependent diffusion coefficients.

Wang and co-workers[23,24] used volume averaged equations and a parabolic profile approximation for solid-phase concentration. This helped reduce the solid-phase partial differential equation to two differential algebraic equations. Their work for Ni–Cd and Ni–MH systems included the addition of an empirical term to take care of the discrepancy in the short-time solution. Along similar lines, Srinivasan et al.[25] used a volume averaged approach for the analysis of thermal behavior of Li-ion cells. However, they did not enumerate when their models fail. The two-parameter model introduced in this paper yields results similar to the parabolic profile model described by Wang and co-workers. It is also noted that the approach developed in this paper can be used to increase the accuracy of the

model by adding parameters, instead of using empirical terms. The performance of the new model is found to be valid even at short times.

In this paper, efficient approximations are developed for the microscale diffusion, which reduce the microscale diffusion (1 PDE) to two or three differential algebraic equations. These approximations are developed by assuming that the solid-state concentration inside the spherical particle can be expressed as a polynomial in the spatial direction.[5] Subramanian et al.[5] developed approximate solutions for solid-phase diffusion based on polynomial profile approximations for constant pore wall flux at the surface of the particle. However, these models cannot be used for battery modeling directly because the pore wall flux at the surface of the particle changes both as a function of time and distance across the porous electrode.

In this paper, approximations are developed for the microscale diffusion for time-dependent pore wall flux. These approximations are then tested with the exact numerical solution of particle diffusion for various defined functions in time for the pore wall flux. Next, these approximations are used with the macroscale model to predict the electrochemical behavior of an Li-ion cell sandwich. The approximations developed reduce the computation time for simulation without compromising accuracy.

Approximate Solution for Microscale Diffusion

Transient diffusion in a spherical electrode particle having an initial concentration c_0 is given by

$$\frac{\partial c}{\partial t} - D_S \frac{1}{r^2} \frac{\partial}{\partial r}\left(r^2 \frac{\partial c}{\partial r}\right) = 0 \qquad [1]$$

Initial and boundary conditions are

$$c = c_0 \text{ at } t = 0 \text{ and for } 0 < r < R_p \text{ (fully charged state)} \quad [2]$$

$$D_s \frac{\partial c_s}{\partial r} = 0 \quad \text{at } r = 0 \text{ and for } t \geqslant 0 \qquad [3]$$

$$D_s \frac{\partial c}{\partial r} = -j_n \quad \text{at } r = R_p \text{ and for } t \geqslant 0 \qquad [4]$$

where j_n is the pore wall flux at the surface of the particle and R_p is the radius of the particle. The pore wall flux is a function of both the distance across the electrode (x) and time (t).[2] Next, we develop approximate solution for Eq. 1 based on polynomial profile approximations developed earlier for constant pore wall flux at the surface.[5]

Two-parameter model.— The concentration profile inside the particle is assumed to be a parabola in r[5-24]

$$c(r,t) = a(t) + b(t)\left(\frac{r^2}{R_p^2}\right) \qquad [5]$$

Substituting Eq. 5 in Eq. 1, we obtain

$$\frac{da(t)}{dt} + \frac{r^2}{R_p^2}\frac{db(t)}{dt} - \frac{6D_S b(t)}{R_p^2} \quad [6]$$

The boundary condition at $r = 0$ is automatically satisfied. The boundary condition at $r = R_p$ (Eq. 4) becomes

$$2\frac{D_S}{R_p}b(t) = -j_n \quad [7]$$

For battery modeling, we are mainly interested in the average concentration (for state of charge) and surface concentration (for electrochemical behavior). Hence, constants $a(t)$ and $b(t)$ are expressed in terms of the volume-averaged concentration $\bar{c}(t)$ and surface concentration $c_S(t)$. The volume-averaged concentration is given by

$$\bar{c}(t) = \int_{r=0}^{R_P} 3\frac{r^2}{R_P^2}c(r,t)d\left(\frac{r}{R_P}\right) \quad [8]$$

Applying Eq. 5 in Eq. 8, we get

$$\bar{c}(t) = a(t) + \frac{3}{5}b(t) \quad [9]$$

Surface concentration c_S is obtained by substituting $r = R_p$ in Eq. 5

$$c_S(t) = a(t) + b(t) \quad [10]$$

Equations 9 and 10 are solved to obtain

$$a(t) = -\frac{3}{2}c_S(t) + \frac{5}{2}\bar{c}(t) \quad [11]$$

$$b(t) = -\frac{5}{2}\bar{c}(t) + \frac{5}{2}c_S(t) \quad [12]$$

The concentration profile given by Eq. 5 is now purely in terms of the volume-averaged concentration $\bar{c}(t)$ and the surface concentration $c_S(t)$

$$c(r,t) = -\frac{3}{2}c_S(t) + \frac{5}{2}\bar{c}(t) + \left(-\frac{5}{2}\bar{c}(t) + \frac{5}{2}c_S(t)\right)\frac{r^2}{R_p^2} \quad [13]$$

We now need two equations to evaluate the average concentration $\bar{c}(t)$ and the surface concentration $c_S(t)$. The volume-averaged concentration can be evaluated by volume averaging the entire governing Eq. 1

$$\int_{x=0}^{R_P} 3\frac{r^2}{R_P^2}\left[\frac{\partial c}{\partial t} - D_S\frac{1}{r^2}\frac{\partial}{\partial r}\left(r^2\frac{\partial c}{\partial r}\right)\right]d\left(\frac{r}{R_P}\right) = 0 \quad [14]$$

Substituting Eq. 12 in Eq. 13 and evaluating, we have

$$\frac{d}{dt}\bar{c}(t) + 3\frac{j_n}{R_p} = 0 \quad [15]$$

The second equation required to evaluate for $c_S(t)$ is obtained by evaluating the boundary condition at $r = R_p$. Evaluating Eq. 5 using Eq. 12, we get

$$\frac{D_s}{R_p}[c_S(t) - \bar{c}(t)] = -\frac{j_n}{5} \quad [16]$$

It is clearly seen that Eq. 14 and 15 are purely in terms of the average concentration and surface concentration. It must be noted here that Eq. 15 and 16 are valid even if the pore wall flux j_n is a function of time.

Higher-order polynomial profile model.— As shown in the previous publication, two-parameter models may not be valid at higher discharge rates.[5,26] In this section, an efficient three-parameter model is now developed.[26] The concentration profile is taken to be

$$c(r,t) = a(t) + b(t)\left(\frac{r^2}{R_p^2}\right) + d(t)\left(\frac{r^4}{R_p^4}\right) \quad [17]$$

Substituting Eq. 17 in Eq. 1 gives

$$\frac{da(t)}{dt} + \frac{r^2}{R_p^2}\frac{db(t)}{dt} + \frac{r^4}{R_p^4}\frac{dd(t)}{dt} - 2\frac{D_S}{R_p^2}\left(3b(t) + 10\frac{r^2}{R_P^2}d(t)\right) = 0 \quad [18]$$

The boundary condition at $r = 0$ is automatically satisfied again. The boundary condition at $r = R_p$ now becomes

$$\frac{2D_S b(t)}{R_p} + \frac{4D_S d(t)}{R_p} = -j_n \quad [19]$$

Next, the constants $a(t)$, $b(t)$, and $d(t)$ are solved in terms volume-averaged concentration $\bar{c}(t)$, surface concentration $c_S(t)$, and volume-averaged concentration flux $\bar{q}(t)$. The volume-averaged concentration flux is a physically meaningful term, which defines the average change of concentration with respect to the position in the system.[26]

Volume-averaged solid-phase concentration can be evaluated using Eq. 8 and is found to be

$$\bar{c}(t) = \frac{3}{7}d(t) + \frac{3}{5}b(t) + a(t) \quad [20]$$

Surface concentration is obtained by evaluating $c(r,t)$ at the surface

$$c_S(t) = a(t) + b(t) + d(t) \quad [21]$$

The volume-averaged concentration flux term is evaluated using the following expression

$$\bar{q}(t) = \int_{r=0}^{R_P} 3\frac{r^2}{R_P^2}\left(\frac{d}{dr}c(r,t)\right)d\left(\frac{r}{R_P}\right) \quad [22]$$

Substituting Eq. 17 in Eq. 22, the average concentration flux is found to be

$$\bar{q}(t) = 2\frac{d(t)}{R_p} + \frac{3}{2}\frac{b(t)}{R_p} \quad [23]$$

Equations 20, 21, and 23 can be solved for constants $a(t)$, $b(t)$, and $d(t)$ in terms of the average concentration $\bar{c}(t)$, the surface concentration $c_S(t)$, and the average concentration flux $\bar{q}(t)$ to obtain

$$a(t) = \frac{39}{4}c_S(t) - 3\bar{q}(t)R_p - \frac{35}{4}\bar{c}(t) \quad [24]$$

$$b(t) = -35c_S(t) + 10\bar{q}(t)R_p + 35\bar{c}(t) \quad [25]$$

$$d(t) = \frac{105}{4}c_S(t) - 7\bar{q}(t)R_p - \frac{105}{4}\bar{c}(t) \quad [26]$$

The concentration profile given by Eq. 17 is now purely in terms of the volume-averaged concentration $\bar{c}(t)$, the volume-averaged concentration flux $\bar{q}(t)$, and the surface concentration $c_S(t)$

$$c(r,t) = \frac{39}{4}c_S(t) - 3\bar{q}(t)R_p - \frac{35}{4}\bar{c}(t) + [-35c_S(t) + 10\bar{q}(t)R_p$$
$$+ 35\bar{c}(t)]\frac{r^2}{R_P^2} + \left(\frac{105}{4}c_S(t) - 7\bar{q}(t)R_p - \frac{105}{4}\bar{c}(t)\right)\frac{r^4}{R_P^4} \quad [27]$$

We now need three equations to solve for the average concentration, the surface concentration, and the average flux. The equation for the volume-averaged concentration is obtained by volume averaging the entire governing Eq. 1 as given by Eq. 14

$$\frac{d}{dt}\bar{c}(t) + 3\frac{j_n}{R_p} = 0 \qquad [28]$$

The second equation for the volume-averaged flux is obtained by volume averaging the differential of the governing equation

$$\int_{x=0}^{R_P} 3\frac{r^2}{R_P^2}\partial\frac{\left[\frac{\partial c}{\partial t} - D_S\frac{1}{r^2}\frac{\partial}{\partial r}\left(r^2\frac{\partial c}{\partial r}\right)\right]}{\partial r}d\left(\frac{r}{R_p}\right) = 0 \qquad [29]$$

Equation 29 yields

$$\frac{d}{dt}\bar{q}(t) + 30\frac{D_S}{R_p^2}\bar{q}(t) + \frac{45}{2}\frac{j_n}{R_p^2} \qquad [30]$$

The third equation can be obtained by evaluating the boundary condition at $r = R_p$ given by Eq. 19

$$35\frac{D_S}{R_p}[c_s - \bar{c}(t)] - 8D_s\bar{q}(t) = -j_n \qquad [31]$$

It is clearly seen that Eq. 28, 30, and 31 are purely in terms of the average concentration, surface concentration and average concentration flux. It must be noted here that the pore wall flux j_n can be a function of time (t).

Note that the approximate equations are developed in dimensional form so that they can be coupled with the governing equations for the macroscale models of batteries. However, to test the accuracy of the approximate models developed, it is convenient to convert the equations to dimensionless form as illustrated in the next section.

Dimensionless Analysis

Equation 1 is converted to dimensionless form using the following dimensionless variables

$$C = \frac{c}{c_0}, \quad z = \frac{r}{R_p}, \quad \text{and } \tau = \frac{D_S t}{R_p^2} \qquad [32]$$

The governing equation in dimensionless form is

$$\frac{\partial C}{\partial \tau} = \frac{1}{z^2}\frac{\partial}{\partial z}\left(z^2\frac{\partial C}{\partial z}\right) \qquad [33]$$

The boundary and initial conditions in dimensionless form are

$$C = 1 \text{ at } \tau = 0 \text{ and for } 0 \leqslant z \leqslant 1 \qquad [34]$$

$$\frac{\partial C}{\partial z} = 0 \text{ at } z = 0 \text{ and for } \tau \geqslant 0 \qquad [35]$$

$$\frac{\partial C}{\partial z} = -\delta(\tau) \text{ at } z = 1 \text{ and for } \tau \geqslant 0 \qquad [36]$$

where $\delta(\tau) = j_n R_p / D_s c_0$ is the dimensionless pore wall flux.

Two-parameter model.— The parabolic profile approximation takes the form

$$C(z,\tau) = a(\tau) + b(\tau)z^2 \qquad [37]$$

Following the procedure described earlier for dimensional equations, the governing equations for volume-averaged dimensionless concentration and surface concentration are obtained as

$$\frac{d}{d\tau}\bar{C}(\tau) + 3\delta(\tau) = 0 \qquad [38]$$

$$C_S(\tau) - \bar{C}(\tau) = -\frac{\delta(\tau)}{5} \qquad [39]$$

Next, to verify the accuracy of the approximations developed, different test functions are tried for the dimensionless pore wall flux $\delta(\tau)$.

Case (i): Linear function $\delta(\tau) = \tau$.—Substituting $\delta(\tau) = \tau$ in Eq. 38 and 39 and solving for the average concentration and the surface concentration in terms of the independent variables time (τ) and position in the system (z), we get

$$\bar{C}(\tau) = 1 - \frac{3\tau^2}{2} \qquad [40]$$

$$C_S(\tau) = 1 - \frac{\tau}{5} - \frac{3\tau^2}{2} \qquad [41]$$

A closed form expression is obtained for the concentration as a function of dimensionless position in the system (z) and dimensionless time (τ)

$$C(z,\tau) = 1 + \frac{\tau}{2}z^2 + \frac{3\tau}{10} - \frac{3\tau^2}{2} \qquad [42]$$

Case (ii): Oscillatory function $\delta(\tau) = sin(\tau)$.—Substituting $\delta(\tau) = sin(\tau)$ in Eq. 38 and 39 and solving for the average concentration and the surface concentration, we get

$$\bar{C}(\tau) = -2 + 3\cos(\tau) \qquad [43]$$

$$C_S(\tau) = -2 - \frac{\sin(\tau)}{5} + 3\cos(\tau) \qquad [44]$$

The concentration profile is obtained as

$$C(z,\tau) = -2 - \frac{\sin(\tau)}{2}z^2 + \frac{3\sin(\tau)}{10} + 3\cos(\tau) \qquad [45]$$

Case (iii): Exponential function $\delta(\tau) = exp(-\tau)$.—Substituting $\delta(\tau) = exp(-\tau)$ in Eq. 38 and 39 and solving for the average concentration and the surface concentration, we get

$$\bar{C}(\tau) = -2 + 3\exp(-\tau) \qquad [46]$$

$$C_S(\tau) - 2 + \frac{14\exp(-\tau)}{5} \qquad [47]$$

The concentration profile is obtained as

$$C(z,\tau) = -2 + \frac{33\exp(-\tau)}{10} - \frac{\exp(-\tau)z^2}{2} \qquad [48]$$

Three-parameter model.— The polynomial profile is taken to be

$$C(z,\tau) = a(\tau) + b(\tau)z^2 + d(\tau)z^4 \qquad [49]$$

Following the procedure described earlier for dimensional equations, the governing equations for volume-averaged dimensionless concentration, volume-averaged dimensionless flux, and surface concentration are obtained as

$$\frac{d}{dt}\bar{C}(\tau) + 3\delta(\tau) = 0 \qquad [50]$$

$$\frac{d}{dt}\bar{Q}(\tau) + 30\bar{Q}(\tau) + \frac{45}{2}\delta(\tau) \qquad [51]$$

$$35[c_s - \bar{c}(t)] - 8\bar{Q}(\tau) = -\delta(\tau) \qquad [52]$$

Next, different test functions are tried for dimensionless pore wall flux $\delta(\tau)$. Only the final equations are reported.
Case (i): Linear function $\delta(\tau) = \tau$.—

$$\bar{C}(\tau) = \frac{3}{2}\tau^2 + 1 \qquad [53]$$

$$\bar{Q}(\tau) = \frac{3}{4}\tau - \frac{1}{40} + \frac{1}{40}\exp(-30\tau) \qquad [54]$$
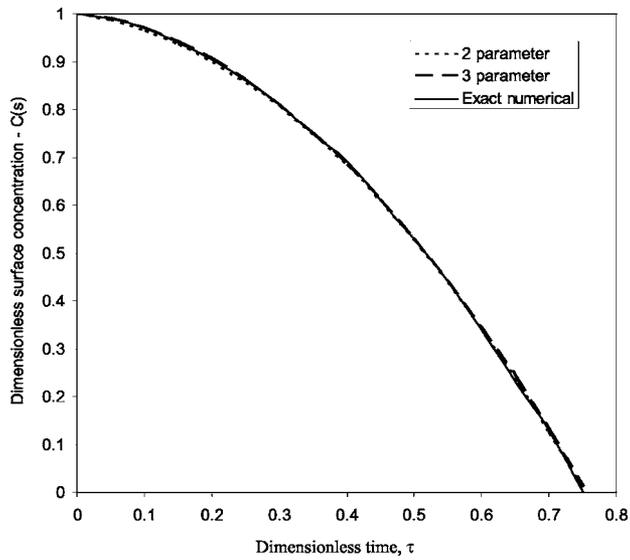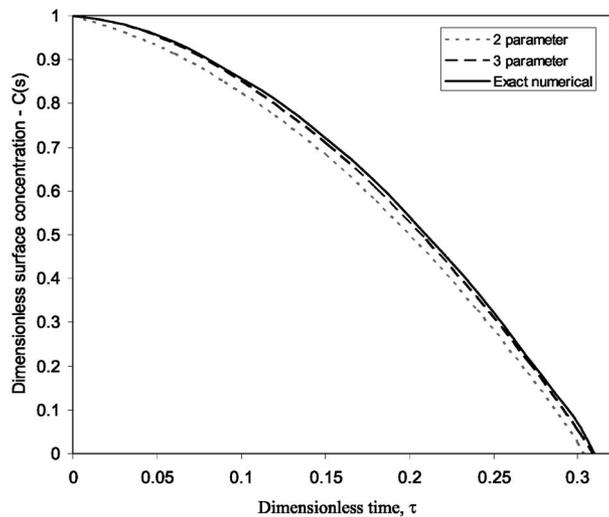
Figure 1. Comparison of approximate models developed for $\delta(\tau) = \tau$.

Figure 3. Comparison of approximate models developed for $\delta(\tau) = 10\tau$.

$$C_S(\tau) = \frac{\tau}{5} + \frac{174}{175} + \frac{1}{175}\exp(-30\tau) + \frac{3}{2}\tau^2 \qquad [55]$$

$$C(z,\tau) = \frac{1427}{1400} + \frac{z^4}{40} + \left(\frac{z^2}{2} - \frac{3}{10}\right)\tau + \frac{3}{2}\tau^2$$
$$+ \left(\frac{1}{20}z^2 - \frac{27}{1400} - \frac{1}{40}z^4\right)\exp(-30\tau) \qquad [56]$$

Case (ii): Oscillatory function $\delta(\tau) = sin(\tau)$.—

$$\bar{C}(\tau) = -3\cos(\tau) + 4 \qquad [57]$$

$$\bar{Q}(\tau) = \frac{675}{901}\sin(\tau) - \frac{45}{1802}\cos(\tau) + \frac{45}{1802}\exp(-30\tau) \qquad [58]$$

$$C_S(\tau) = 4 + \frac{6301}{31535}\sin(\tau) + \frac{36}{6307}\exp(-30\tau) - \frac{18957}{6307}\cos(\tau)$$
$$[59]$$

$$C(z,\tau) = 4 + \left(\frac{449}{901}z^2 + \frac{3}{3604}z^4 - \frac{37761}{126140}\right)\sin(\tau)$$
$$+ \left(\frac{45}{1802}z^4 - \frac{37599}{12614} - \frac{45}{901}z^2\right)\cos(\tau)$$
$$+ \left(\frac{45}{901}z^2 - \frac{243}{12614} - \frac{45}{1802}z^4\right)\exp(-30\tau) \qquad [60]$$

Case (iii): Exponential function $\delta(\tau) = exp(-\tau)$.—

$$\bar{C}(\tau) = -3\exp(-\tau) + 4 \qquad [61]$$

$$\bar{Q}(\tau) = \frac{45}{58}\exp(\tau) - \frac{45}{58}\exp(-30\tau) \qquad [62]$$

$$C_S(\tau) = 4 - \frac{36}{203}\exp(-30\tau) - \frac{2836}{1015}\exp(-\tau) \qquad [63]$$

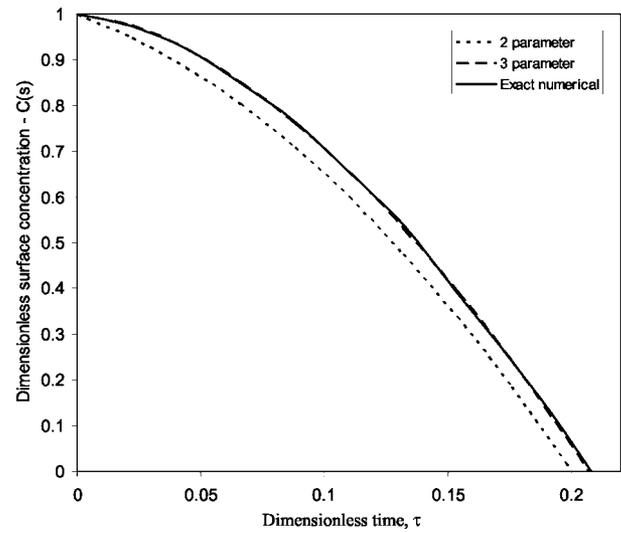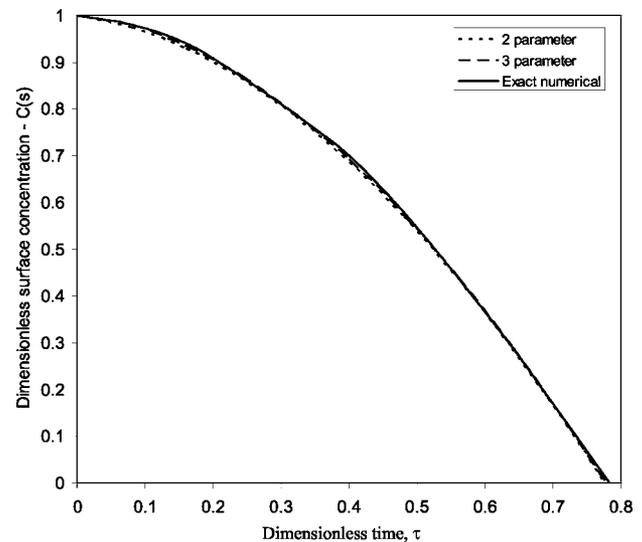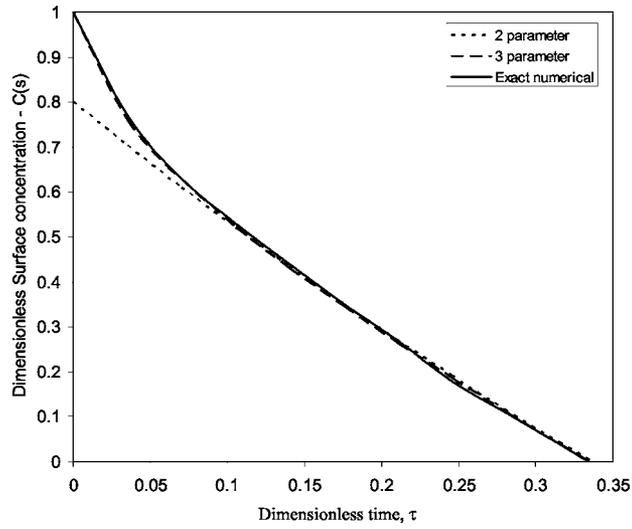**Figure 2.** Comparison of approximate models developed for $\delta(\tau) = 5\tau$.

Figure 4. Comparison of approximate models developed for $\delta(\tau) = \sin(\tau)$.

Figure 5. Comparison of approximate models developed for $\delta(\tau)$ = exp($-\tau$).

Figure 6. Lithium-ion cell sandwich, consisting of lithium-foil, separator, and porous electrode.

$$C(z,\tau) = 4 + \left(\frac{16}{29}z^2 - \frac{3}{116}z^4 - \frac{13479}{4060}\right)\exp(\tau)$$

$$+ \left(\frac{243}{406} - \frac{45}{29}z^2 + \frac{45}{58}z^4\right)\exp(-30\tau) \qquad [64]$$

Accuracy of approximate models.— Electrochemical behavior is governed by the surface concentration. Hence, the accuracy of the approximate models developed is verified by plotting the dimensionless surface concentration. To compare the accuracy, a rigorous numerical solution is obtained by solving Eq. 33 subject to boundary conditions/initial conditions given by Eq. 34-36 using numerical method of lines.[17,18] The exact numerical solution is obtained by applying finite differences in the spatial direction and by integrating the resulting system of coupled ordinary differential equations numerically in time. Twenty node points were found to be sufficient for the purpose of this paper.
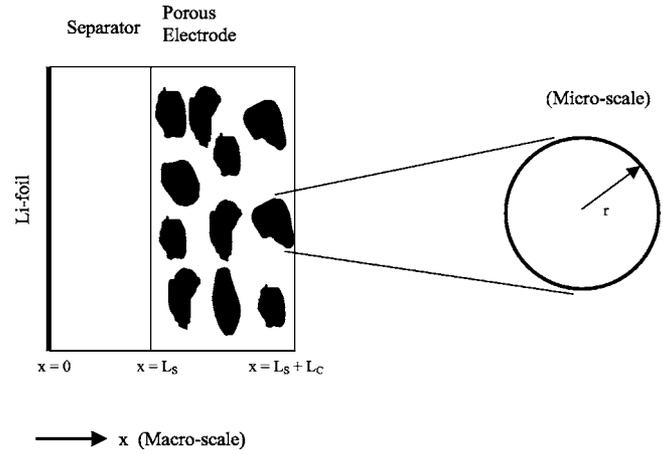
In Fig. 1, dimensionless surface concentration is plotted as a function of dimensionless time τ for a linear function for the dimensionless pore wall flux, $\delta(\tau) = \tau$. From Fig. 1, we conclude that both two- and three-parameter models fit exactly with the exact numerical solution for the linear function of time τ.

In Fig. 2, dimensionless surface concentration is plotted as a function of dimensionless time τ for a linear function for the dimensionless pore wall flux, $\delta(\tau) = 5\tau$. From Fig. 2, we conclude that the three-parameter models fit better than the two-parameter model with the numerical exact model for the linear function of time 5τ. The increase in magnitude causes the two-parameter model to show a small deviation.

In Fig. 3, dimensionless surface concentration is plotted as a function of dimensionless time τ for a linear function for the dimensionless pore wall flux, $\delta(\tau) = 10\tau$. From Fig. 3, we conclude that the three-parameter models fit better than the two-parameter model with the numerical exact model for the linear function of time 10τ. The increase in magnitude causes the two-parameter model to pre-

Table I. Summary of model equations and boundary equations in the macroscale.

Variables	Equations	Boundary condition
Separator		At $x = 0$
c_2	$\dfrac{\partial c_2}{\partial t} = D\varepsilon_S^{0.5}\dfrac{\partial^2 c_2}{\partial x^2}$	$D\dfrac{\partial c_2}{\partial x} = -\dfrac{i_{app}(1 - t^+)}{\varepsilon_S^{1.5}F}$
φ_2	$\dfrac{\partial^2 \varphi_2}{\partial x^2} - \dfrac{\partial}{\partial x}\left(\dfrac{2RT(1 - t^+)}{F}\dfrac{\partial \ln c_2}{\partial x}\right) = 0$	$\varphi_2 = 0$
Composite cathode		At $x = L_s + L_c$
φ_1	$\dfrac{\partial^2 \varphi_1}{\partial x^2} = \dfrac{aFj_n}{\sigma_k}$	$\dfrac{\partial \varphi_1}{\partial x} = -\dfrac{i_{app}}{\sigma}$
φ_2	$\dfrac{\partial^2 \varphi_2}{\partial x^2} - \dfrac{\partial}{\partial x}\left(\dfrac{2RT(1 - t^+)}{F}\dfrac{\partial \ln c_2}{\partial x}\right) = -\dfrac{aFj_n}{\kappa_{eff}}$	$\dfrac{\partial \varphi_2}{\partial x} = 0$
c_2	$\varepsilon_p\dfrac{\partial c}{\partial t} = D\varepsilon_P^{1.5}\dfrac{\partial^2 c}{\partial x^2} + aj_n(1 - t^+)$	$\dfrac{\partial c_2}{\partial x} = 0$

$$j_n = K(c_{max} - c)^{\alpha_c}c^{\alpha_a}\left[\exp\left(\frac{\alpha_a F(\varphi_1 - \varphi_2 - U)}{RT}\right) - \exp\left(-\frac{(1 - \alpha_c)F(\varphi_1 - \varphi_2 - U)}{RT}\right)\right]$$

$$U = \frac{4.707 - 36.129\left(\frac{c_s}{c_T}\right) + 104.813\left(\frac{c_s}{c_T}\right)^2 + 149.491\left(\frac{c_s}{c_T}\right)^3 + 111.818\left(\frac{c_s}{c_T}\right)^4 - 35.705\left(\frac{c_s}{c_T}\right)^5}{1 - 7.598\left(\frac{c_s}{c_T}\right) + 21.779\left(\frac{c_s}{c_T}\right)^2 - 30.959\left(\frac{c_s}{c_T}\right)^3 + 23.632\left(\frac{c_s}{c_T}\right)^4 + 7.8474\left(\frac{c_s}{c_T}\right)^5}$$

Table II. Values for various parameters for LiCoO$_2$.

Parameters	Value	Parameters	Value
D_s	1.0×10^{-13}	T	100°C
D	7.5×10^{-10}	L_s	23 μm
i_{app}	60 A/m^2	L_c	92 μm
α_a, α_c	0.5	c^0	1000 mol/m^3
c_T	51554 mol/m^3	ε_s	0.724
K	2.45×10^{-6} m^4/mol s	ε_p	0.39
c_{max}	51554		
σ	100 S/m		

dict erroneous results. Further increase in the magnitude causes the two-parameter model to deviate further from the exact numerical model.

In Fig. 4, dimensionless surface concentration is plotted as a function of dimensionless time τ for a linear function for the dimensionless pore wall flux, $\delta(\tau) = \sin(\tau)$. From Fig. 4, we can infer that both two- and three-parameter models fit exactly with the numerical exact model for a sinusoidal function in time.

In Fig. 5, dimensionless surface concentration is plotted as a function of dimensionless time τ for a linear function for the dimensionless pore wall flux, $\delta(\tau) = \exp(-\tau)$. We observe that the two-parameter model fails at very low values of time. The three-parameter model shows good fit to the exact numerical model at all the values of state of charge. It is interesting to note, however, that the two-parameter model shows good fit to the exact numerical model at high values of time.

From Fig. 1-5 we can conclude that three-parameter models can be used safely without compromising the accuracy. Also, two-parameter models can be used as long as $\delta \leq 1$. Also, even for higher values of δ, two-parameter models can be used at long times. In addition, two parameters work if δ starts from zero. This observation is useful for battery modeling because pore wall flux is zero before the beginning of discharge. After the discharge begins, the pore-wall flux inside the porous electrode increases with time. The approximate models developed for the microscale diffusion are coupled with the macroscale equations to predict the electrochemical behavior of an Li-ion cell sandwich in the next section.

Electrochemical Behavior of an Li-Ion Cell Sandwich

In the previous sections, approximate models were developed for microscale diffusion of ions inside a spherical particle. The approximate models developed convert one PDE to two or three differential algebraic equations. The approximate models developed were then validated by comparing with the exact numerical solution. If one has to solve just one PDE inside the particle, then one can get a closed-
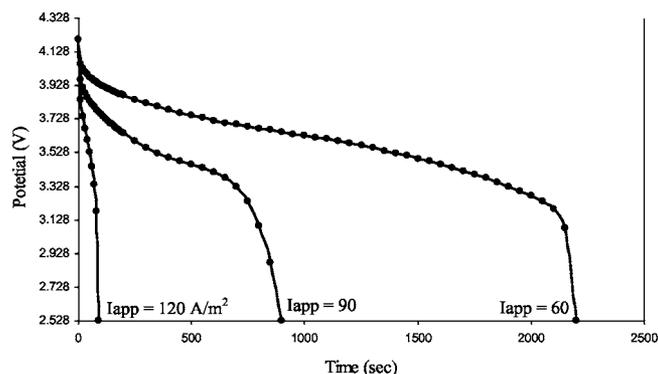
Figure 7. Potential obtained by using an approximate model for the solid phase concentration is compared with potential obtained by using 20 nodes in the particles. Solid line represents the node model (rigorous solution) and solid dots represent the approximate model.
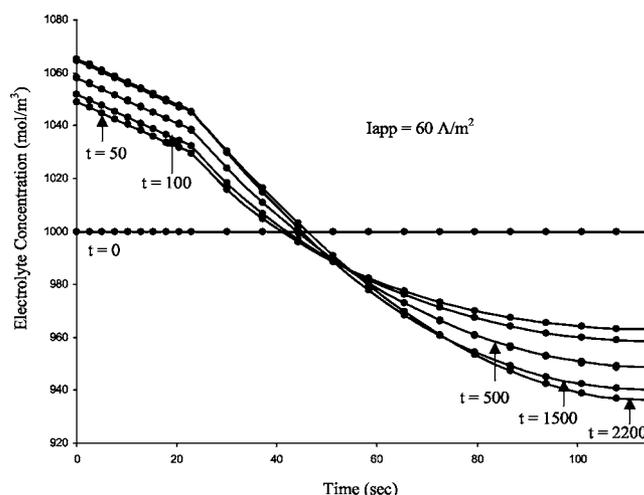
Figure 8. Electrolyte concentration inside the cell sandwich predicted using an approximate model for the solid phase concentration is compared with electrolyte concentration obtained using 20 nodes in the particles. Solid line represents the node model (rigorous solution) and solid dots represent the approximate model.

form solution or a numerical solution quite easily.[27-30] The approximate models developed, though accurate, are not needed if one has to solve just a single PDE. However, for battery modeling, a single PDE for the microscale diffusion is coupled with other PDEs in the macroscale.[2,3] Next, we show the utility of the approximate models developed for battery modeling.

The geometry modeled is shown in Fig. 6.[2] The Li-ion cell sandwich modeled consists of lithium foil, a separator, and a porous electrode. The governing equations and boundary conditions for the in the macroscale are listed in Table I. The typical values of the constants are given in Table II. There are two PDEs in the separator and three PDEs in the porous electrode.[2,3] In addition, for the porous electrode, the solid-phase diffusion is solved inside the particle in the pseudodirection r (microscale) (Eq. 1-4).

For simulation purposes, the governing equations in the macroscale are discretized in the x direction using 100 node points in the separator and 100 node points in the porous electrode. For a rigorous numerical solution, if 20 node points are used inside the particle in the microscale, then we have $4 \times 100 \times 20 = 8000$ differential algebraic equations in the porous electrode.[2,3] When our approximate model (Eq. 15 and 16) is used for the microscale diffusion, we have $4 \times 100 \times 2 = 800$ differential algebraic equations in the porous electrode. Both the rigorous numerical solution (with rigorous solution of particle diffusion) and the numerical solution with approximate models for the particle diffusion are compared in Fig. 7. We observe that the approximate model for the particle diffusion matches exactly with the rigorous simulation. In addition, we observe that the approximate model developed in this paper predicts the electrolyte concentration and solid-phase concentration inside the porous electrode accurately, as shown in Fig. 8 and 9.

Rigorous solution to predict one discharge curve with numerical discretization of micro- and macroscale models takes around 2 min in a 2.6 GHz processor. Numerical solution with the approximate model for the microscale developed takes only 10 s to predict one discharge curve. Discharge curves are compared for applied current density 60, 90, and 120 A/m^2. Note that higher-order polynomial models (Eq. 28, 30, and 31) predict the same behavior. The two-parameter model is found to be sufficient for this system. However, for porous electrodes with high values of pore wall flux or very low solid-phase diffusion coefficients, one might need three-parameter models. Also, because it is expensive to get a rigorous numerical solution, the best option is to simulate the behavior using both two-parameter and three-parameter models for the highest possible ap-
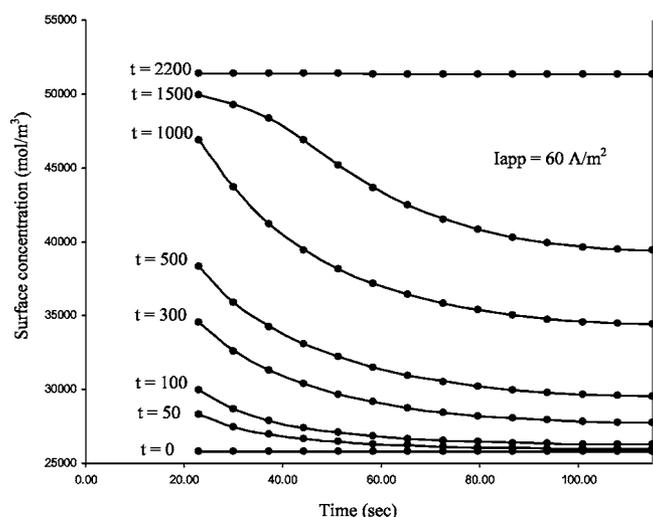
Figure 9. Solid-phase surface concentration at the particle/electrolyte interface inside the cell sandwich predicted using an approximate model (for the solid phase concentration) is compared with solid-phase surface concentration obtained using 20 nodes in the particles. Solid line represents the node model (rigorous solution) and solid dots represent the approximate model.

plied current and see if they match. If they match, then one can safely use the two-parameter models even for pulse currents, voltammetry, and other complicated boundary conditions, geometry, and systems.

In this paper, approximations were developed and implemented only for microscale diffusion in spherical particles. However, the same methodology has been used by the authors for cylindrical and rectangular particles with the same effect. The simplified equations are very similar to the simplified equations for the spherical particle (Eq. 15, 16, 29, 31, and 32) and are available upon request from the corresponding author.

Currently, we are working on developing optimized two-parameter and three-parameter models for various electrochemical systems for both macroscale and microscale phenomena.

Conclusions

In this paper, approximate models were developed for solid-phase diffusion in the microscale. The approximate models developed were tested for arbitrary functions of pore wall flux. In addition, the approximate models developed were then used to predict the discharge curves of a lithium-ion cell sandwich consisting of a lithium foil, separator, and porous electrode. The approximate models developed save computation time by more than 80% without compromising accuracy.

In this paper, the utility of the approximate models developed was shown for one porous electrode only. The same concept can be directly extended to predict the electrochemical behavior of lithium-ion batteries with two porous intercalation electrodes. In addition, similar approximate models have been found to be of use in predicting the electrochemical behavior of PEM fuel cells and will be published later.

Note that the approximate models developed (Eq. 15, 16, 29, 31, and 32) are valid even if the solid-state diffusion coefficient is a function of solid-state concentration. This will be discussed in a later publication. The approximate models developed in this paper are found to be useful in predicting the impedance response of Li-ion batteries also and will be communicated later.

Acknowledgments

List of Symbols

$a(t), b(t), d(t)$	time-dependent constants in the polynomial approximations
c_2	concentration of electrolyte (mol/m^3)
c	solid-phase concentration (mol/m^3)
c_s	solid-phase concentration at the surface of the particle (mol/m^3)
C	dimensionless solid-phase concentration
r	distance from the center of the particle (m), microscale
t	time (s)
x	distance (m), macroscale
D	diffusion coefficient of the electrolyte (m^2/s)
D_s	diffusion coefficient of the electrolyte in the solid particles (m^2/s)
a	interfacial area (m^{-1})
j_n	pore wall flux of Li ions (mol/m^2/s)
t^+	transfer number
i_{app}	current density (A/m^2)
L_c, L_s	length of the electrode (m), length of the separator (m)
F	Faraday's law constant (96,487 C/mol)
n	number of electrons transferred ($n = 1$ for the simulation)
cs_{av}	average concentration in the solid particle

Greek

ε_p	porosity of the electrode
ε_s	porosity of the separator
φ_1	solid phase potential
φ_2	solution phase potential
κ	electrolyte conductivity (S/m)
σ	ionic conductivity (S/m)

References

1. J. S. Newman, *Electrochemical Systems*, Prentice Hall, Englewood Cliffs, NJ (1991).
2. M. Doyle, T. F. Fuller, and J. Newman, *J. Electrochem. Soc.*, **140**, 1526 (1993).
3. G. G. Botte, V. R. Subramanian, and R. E. White, *Electrochim. Acta*, **45**, 2595 (2000).
4. M. Doyle, J. Newman, A. S. Gozdz, C. N. Schmutz, and J. M. Tarascan, *J. Electrochem. Soc.*, **143**, 1890 (1996).
5. V. R. Subramanian, J. A. Ritter, and R. E. White, *J. Electrochem. Soc.*, **148**, E444 (2001).
6. C. H. Liaw, J. S. P. Wang, R. H. Greenkorn, and K. C. Chao, *AIChE J.*, **54**, 376 (1979).
7. N. Wakao and S. Kaguei, *Heat and Mass Transfer in Packed Beds*, Gordon & Breach, New York (1982).
8. D. Do and R. Rice, *AIChE J.*, **32**, 149 (1986).
9. J. H. Hills, *Chem. Eng. Sci.*, **11**, 2779 (1986).
10. D. Do and P. L. J. Mayfield, *AIChE J.*, **33**, 1397 (1987).
11. T. Tomida and B. J. McCoy, *AIChE J.*, **33**, 1908 (1987).
12. D. Do and T. Nguyen, *Chem. Eng. Commun.*, **72**, 171 (1988).
13. M. A. Buzanowski and R. T. Yang, *Chem. Eng. Sci.*, **44**, 2683 (1989).
14. D. H. Kim, *AIChE J.*, **35**, 343 (1989).
15. M. Goto, J. M. Smith, and B. J. McCoy, *Chem. Eng. Sci.*, **45**, 443 (1990).
16. C. C. Lai and C. S. Tan, *AIChE J.*, **37**, 461 (1991).
17. M. Goto and T. Hirose, *Chem. Eng. Sci.*, **48**, 443 (1993).
18. C. Yao and C. Tien, *Chem. Eng. Sci.*, **48**, 187 (1993).
19. R. Zhang and J. A. Ritter, *Chem. Eng. Sci.*, **52**, 3161 (1997).
20. G. Carta and A. Cincotti, *Chem. Eng. Sci.*, **53**, 3483 (1998).
21. G. G. Botte, R. Zhang, and J. A. Ritter, *Chem. Eng. Sci.*, **53**, 4135 (1998).
22. G. G. Botte, R. Zhang, and J. A. Ritter, *Adsorption*, **5**, 375 (1999).
23. C. Y. Wang, W. B. Gu, and B. Y. Liaw, *J. Electrochem. Soc.*, **145**, 3407 (1998).
24. W. B. Gu, C. Y. Wang, and B. Y. Liaw, *J. Electrochem. Soc.*, **145**, 3418 (1998).
25. V. Srinivasan and C. Y. Wang, *J. Electrochem. Soc.*, **150**, A98 (2003).
26. V. R. Subramanian, *Chem. Eng. Sci.*, To be submitted.
27. V. R. Subramanian and R. E. White, *J. Power Sources*, **96**, 385 (2001).
28. H. S. Carslaw and J. C. Jaeger, *Conduction of Heat in Solids*, Oxford University Press, London (1973).
29. A. Varma and M. Morbidelli, *Mathematical Methods in Chemical Engineering*, Oxford University Press, New York (1997).
30. V. R. Subramanian and R. E. White, *Chem. Eng. Edn.*, **34**, 328 (2000).